10/4/18/89 gs (1)

# SANDIA REPORT

SAND88—2768 • UC—
Unlimited Release 700
Printed February 1989

# Causes and Control of Gas Precompression Effects on the 25-Meter Helium/Air Gun

M. B. Boslough, R. E. Setchell, M. U. Anderson,
M. R. Lewis, D. E. Wackerbarth

**Prepared by**
**Sandia National Laboratories**
**Albuquerque, New Mexico 87185 and Livermore, California 94550**
**for the United States Department of Energy**
**under Contract DE-AC04-76DP00789**

---

Issued by Sandia National Laboratories, operated for the United States Department of Energy by Sandia Corporation.



Printed in the United States of America
Available from
National Technical Information Service
U.S. Department of Commerce
5285 Port Royal Road
Springfield, VA 22161

NTIS price codes
Printed copy: A03
Microfiche copy: A01

SAND88-2768
Unlimited Release
Printed February 1989

Distribution
Category UC
700

SAND--88-2768

DE89 009716

# CAUSES AND CONTROL OF GAS PRECOMPRESSION EFFECTS ON THE 25-METER HELIUM/AIR GUN

M. B. Boslough, R. E. Setchell, M. U. Anderson,
M. R. Lewis, and D. E. Wackerbarth+
Sandia National Laboratories
Albuquerque, NM 87185

## ABSTRACT

Recent experiments making use of quartz stress gauges and radiation pyrometry on the Sandia 25-meter gas gun have shown that, under certain circumstances, gas becomes trapped between the projectile and target and can generate elevated pressures and temperatures in the target before impact. The presence of high temperature compressed gases can lead to a number of other deleterious effects, including ignition of reactive materials, shorting of triggering pins, and interference with light-emission measurements. We have now shown that the gas precompression effect on the target is due primarily to blowby of compressed driver gases past the projectile. By modifying the design of some projectiles, making a minor change in the breech, and changing the starting position of the projectile in the barrel, we can eliminate any significant gas precompression effects on the target. For applications in which precompression is desired, we have found that this effect can be reproducibly controlled. Possible applications include quasi-isentropic compression, light generation for transmission spectroscopy, and adjustment of conditions for shock-induced chemical reactions.

+ Ewing Corporation

TABLE OF CONTENTS

Page



TABLES



FIGURES

# I. Introduction

The Sandia 25-meter compressed gas gun was designed to accelerate precisely aligned, flat-faced projectiles over a large velocity range with a minimum of air-cushioning effects [1]. The gun is capable of firing 63 mm diameter projectiles with masses between 0.25 and 5 kg over a continuous range of velocities from 0.03 to 1.6 km/sec [2]. Gas sealing between the aluminum projectiles and the barrel wall is achieved with nitrile (Buna-N: Parker Seals #N674-70) O-rings and teflon backup rings. During gun operations, a projectile is placed at the breech end of the barrel and the space behind it evacuated to avoid pressure differentials that could force the projectile down the barrel before firing. The barrel is then evacuated to a pressure of about 20 mm (Hg) in order to reduce drag and minimize the air cushioning. The breech is then filled with either air or helium to a pressure of up to 35 MPa. Sudden release of the driver gas is accomplished using either a wrap-around breech or a double-diaphragm rupture assembly. The high pressure gas then accelerates the projectile through the 25-meter barrel, while the O-rings prevent gas blowby, until the projectile reaches the muzzle where it impacts a target.

The intent of the gun design was to achieve a condition as close as possible to the ideal case of an instantaneous step function in compressive stress over a significant area of the impact interface. In practice, however, the gun barrel cannot be

perfectly evacuated. As a result, the residual barrel gas is shock-compressed by the accelerating projectile, and multiple shock reverberations can produce significant pressures at the target before impact. Thus, if the barrel is poorly evacuated, a number of undesirable effects can arise. First, the arrival of gas shock waves at the target before impact will lead to preliminary wave motion through the target assembly, resulting in an effective initial state that may be significantly different than that desired or expected. Second, high-temperature gases in contact with the surface of the target may ignite reactive materials that would otherwise remain unreacted under shock. Third, if the shocked gas is ionized, unprotected time-of-arrival pins can trigger prematurely. Finally, the light emission from the compressed gas can interfere with experimental efforts to measure light emission from the shocked target. Setchell and Guzman [3] showed that under normal firing conditions the barrel vacuum was sufficiently good to ameliorate the above listed problems.

Recently, attempts to achieve the highest possible impact velocities have resulted in minor modifications or variations to gun operations that have had the cumulative effect of compromising the amount of air cushioning that takes place just before impact under certain conditions. The consequent precompression was first observed in a VISAR-measured particle-velocity history of the impact interface under the conditions for maximum impact velocity (Fig. 1). The effects of precompression

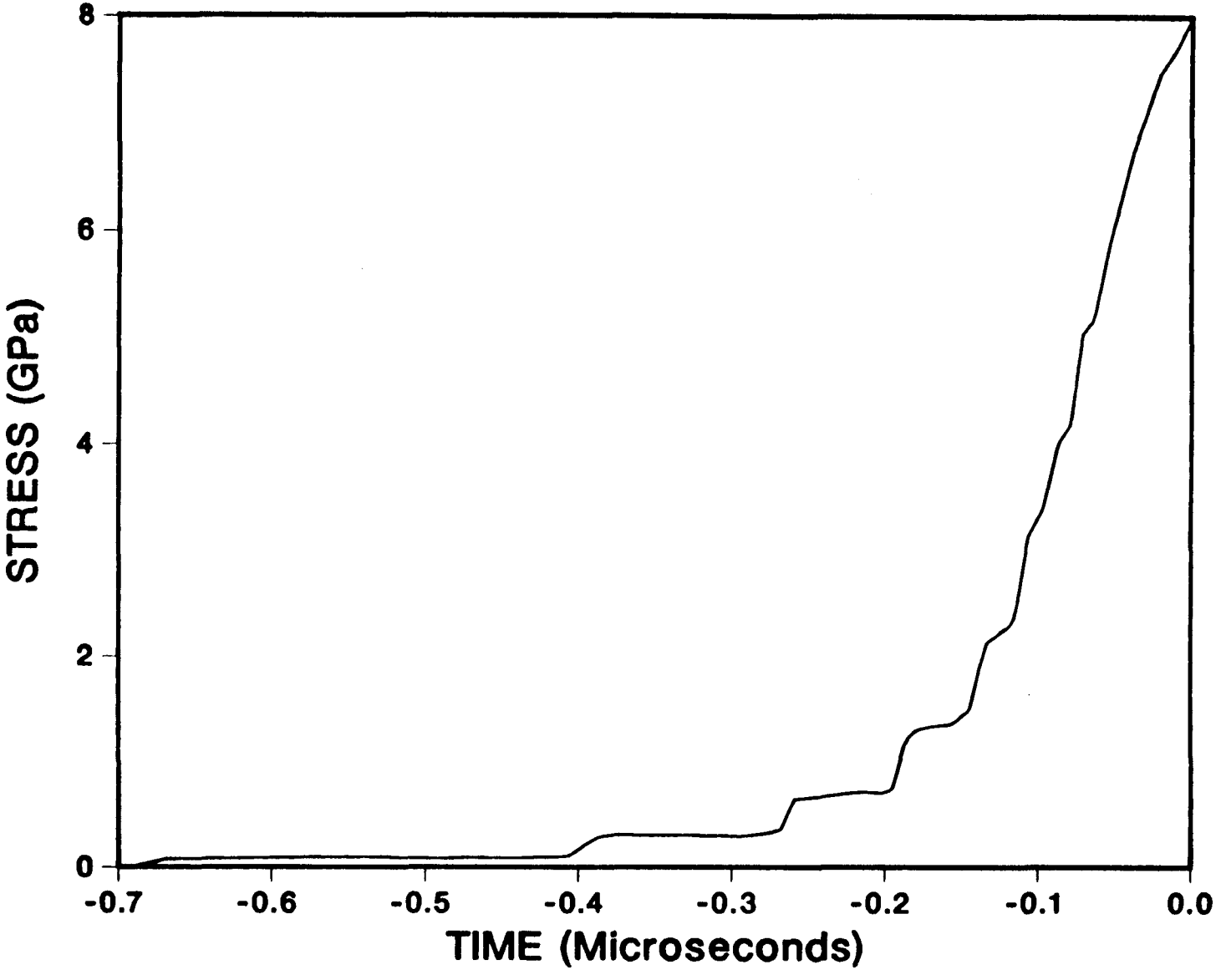


Fig. 1 VISAR record for experiment 2168, reverse impact of HNS on sapphire at 1.33 km/sec. The shock-Hugoniot relation for sapphire has been used to convert particle velocity to axial stress. Impact occurs at t = 0.

were also observed by using full-electrode, shunted quartz gauges (Fig. 2) and by radiation pyrometry during high-velocity experiments. The present paper describes the modifications and variations that resulted in the precompression effect, a series of experiments carried out to observe and troubleshoot the problem, and the measures that were taken to prevent or control it. Our findings are summarized in Table 1. We also suggest a number of applications for which controlled precompression would be desired, and propose a method by which the precompression can be tailored for a given application.

## II. Relevant Details of Gun Design

Before describing the modifications and variations that had an effect on the amount of gas cushioning, the gun is described in its standard mode of operation. In Figure 3, the various types of projectiles we used are illustrated in cross-section. Figure 4 shows the most commonly used ("standard") projectile in its normal position in the breech just prior to firing. This aluminum projectile has a nominal mass of 0.84 kg. Ideally, during gun operations, it is inserted sufficiently far into the barrel of the gun so that both sets of O-rings seal against the inner wall. Since the projectile is loaded under standard atmospheric conditions, one atmosphere of air is trapped in the annular region between the outer diameter of the projectile

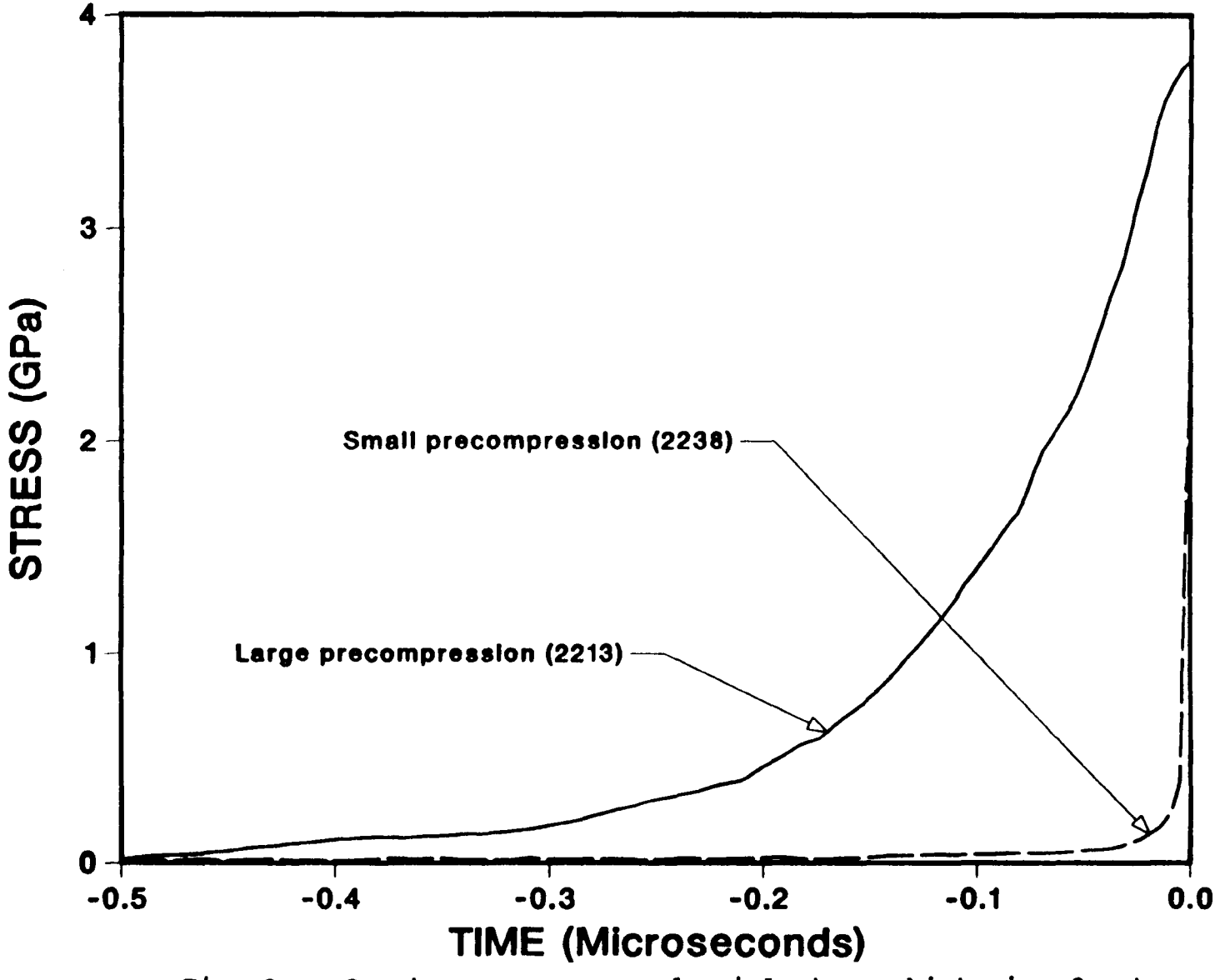


Fig. 2 Quartz gauge-measured axial stress histories for two experiments: one with a large precompression (2213), and the other with small precompression (2238). The only difference in firing conditions was the initial projectile position (see Table 1). Impact at t = 0.

Table 1. Causes and Controls for Gas Precompression Effects

| | Causes | Controls |
|---|---|---|
| 1. | Residual barrel gas due to partial vacuum before firing. | Improve vacuum system. |
| 2. | Gas trapped between O-rings and released when front O-ring clears end of 63 mm barrel prior to impact. | Modify loading procedure (change initial position of projectile). Modify projectile (increase diameter). |
| 3. | Gas released past O-rings due to plugged 6.35 mm port in barrel wall. | Reduce diameter of port. |
| 4. | Propellant gas released past rear projectile O-ring. | Modify projectile design (increase length) and/or reduce length of target spacer. |

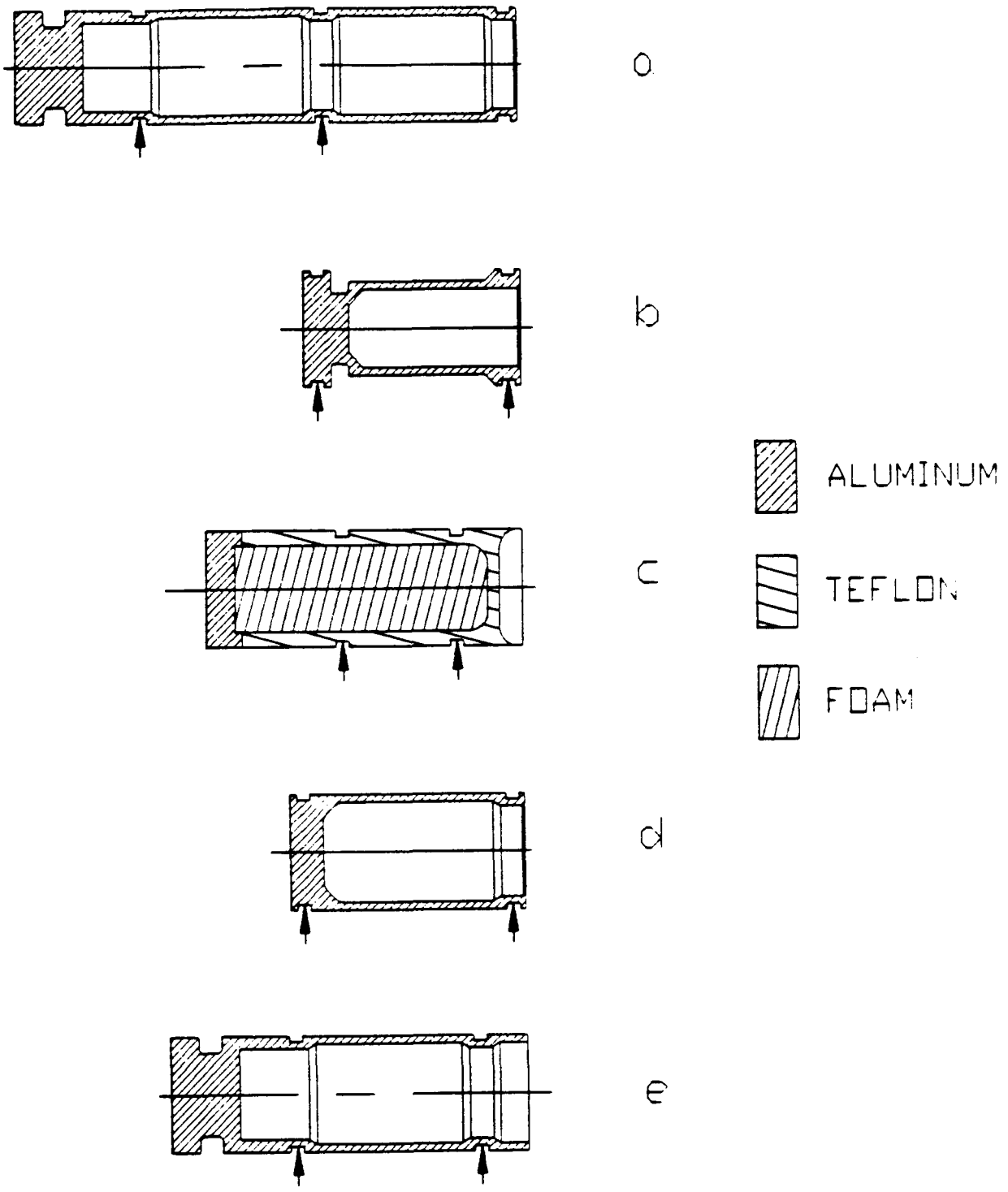


Fig. 3 Cross sections of projectiles: a) "standard", b)"narrow high-velocity", c) "teflon", d)"wide high-velocity", and e) "shortened standard". Small arrows indicate positions of O-rings.

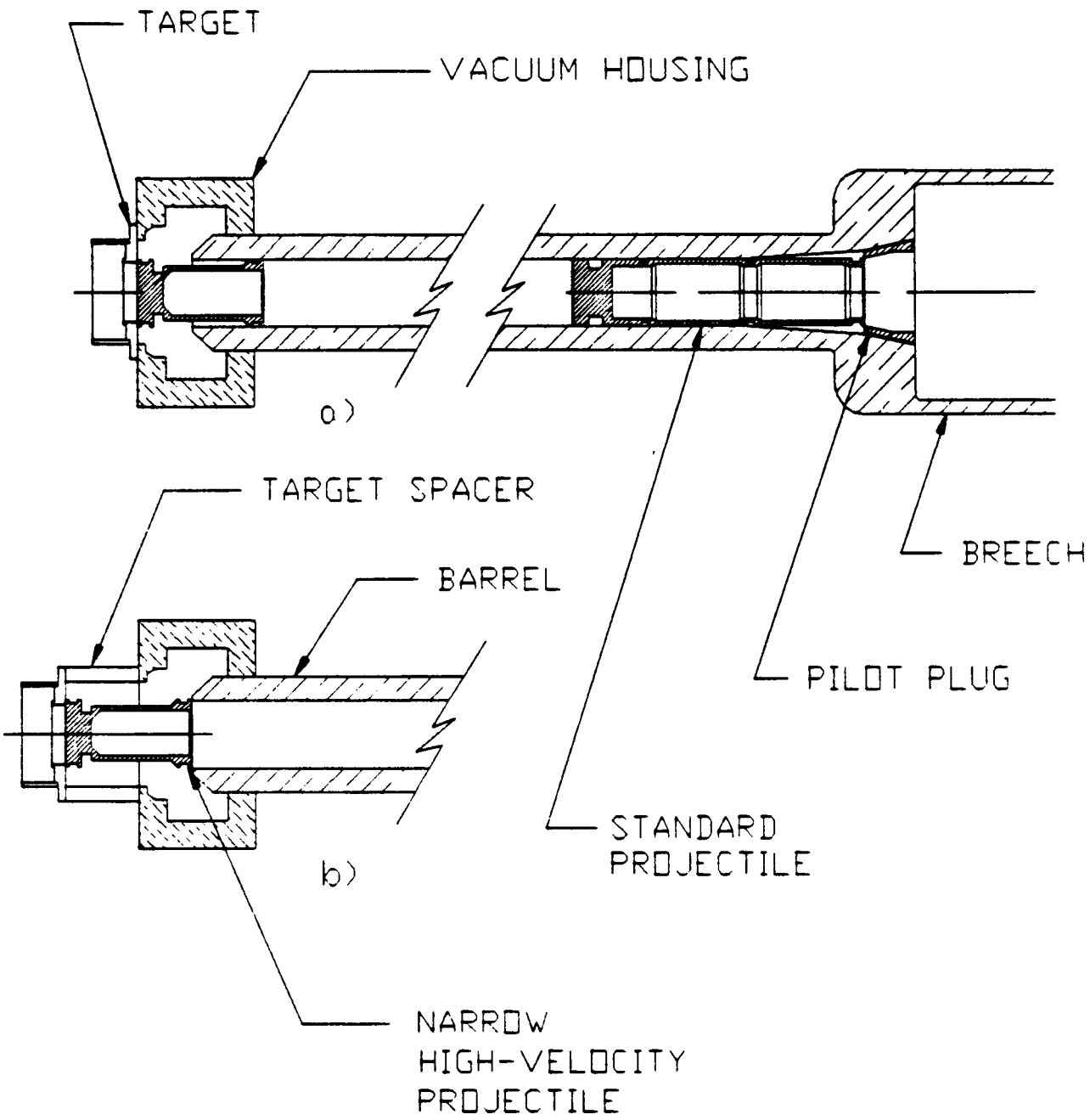


Fig. 4 (a) Configuration of gun with standard projectile in breech. Length of projectile prevents high-pressure driver gas from getting into space between O-rings. A "narrow high-velocity" projectile is shown at the muzzle with no spacer in place; the rear O-ring still seals at the time of impact. (b) Muzzle of gun with spacer in place. Rear O-ring of narrow high-velocity projectile is outside the barrel at impact.

(62.56 mm) and the inner diameter of the barrel (62.74 mm) between the O-rings. This region where gas can be trapped will henceforth be referred to as the "projectile void". The total volume of air in the projectile void between the two O-rings (101.6 mm apart) is 1.8 $cm^3$. This amount of gas is equal to that which would fill the entire barrel volume to 18 mm (Hg), a vacuum similar to what is attained prior to an experiment. If the forward O-ring fails during projectile motion, the small amount of gas initially between the O-rings can contribute to precompression. If the forward O-ring remains intact until impact, then when the projectile passes through the 60-mm-long expanded part of the barrel (the vacuum housing; Fig. 4a) very little gas will be able to get around it.

One variation to gun operations makes use of an optional target mounting spacer that effectively extends the expanded part of the barrel another 63.5 mm, There are two reasons for this optional spacer: 1) to prevent muzzle damage during experiments on high-explosives, and 2) to allow the targets to be mounted closer to the axis of the surrounding chamber's optical port, which is used for VISAR, optical spectroscopy, streak and framing photography, and pyrometry experiments. This modification consists of an expendable 63.5 mm-long spacer which is mounted between the muzzle and the standard target cup (see Fig. 4b). This spacer allows more time for gases to blow past the front O-ring of the projectile and contribute to precompression. However, when the standard projectile is used with the target in

this configuration, the rear O-ring remains in the barrel until the time of impact, so that driver gases are never allowed to escape. We have not observed a significant precompression problem using this spacer with standard projectiles.

Recently, we have begun using lighter projectiles to attain higher impact velocities for a given breech pressure. In Figure 3, the "narrow high-velocity" projectile (b) is compared to the standard version (a). Because the rear O-ring is closer to the impact face of the projectile (116 as opposed to 175 mm), this rear O-ring leaves the muzzle end of the barrel when the projectile face still has 8 mm to travel before impact, when the optional spacer is used. Thus, in principle, the driver gas that had been sealed by the rear O-ring has time during which it can pass around the projectile unhindered.

If blowby of breech gas due to O-ring position were the only problem, the simple solution would be to increase the length of the projectile. Unfortunately a much stronger, additional effect is related to the way in which the projectile is loaded into the breech end of the barrel. Figure 5a shows a narrow high velocity projectile in its initial position in the breech before firing. The position of the tail end is determined by the breech pilot plug, and is the same as that for the standard projectile (Fig. 4a). However, because the narrow high-velocity projectile is much shorter, the rear O-ring extends well into the breech taper. Consequently, high-pressure driver gas is injected into the space between the O-rings during the time interval between diaphragm

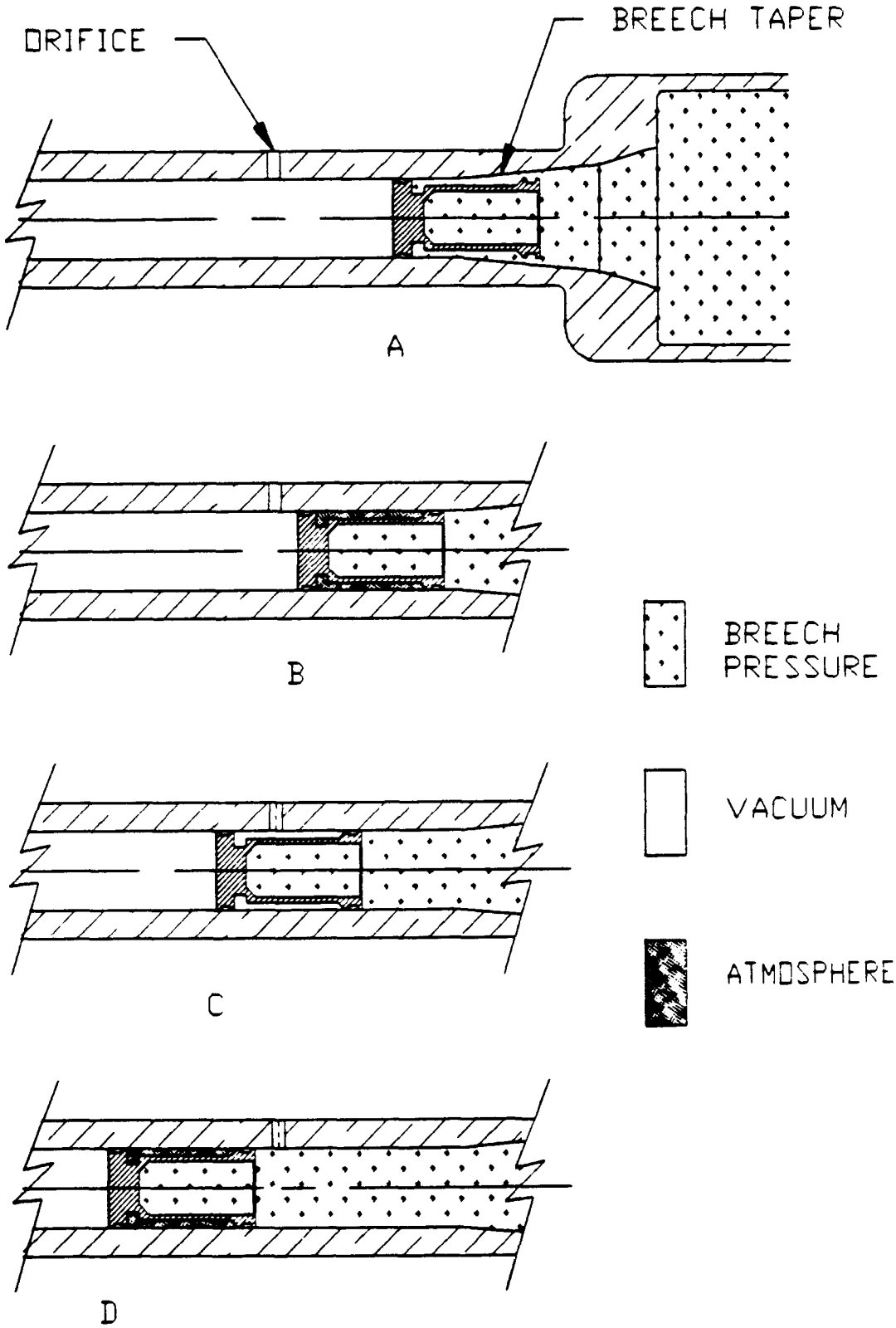


Fig. 5 Cross-section of breech end of barrel, with four initial starting positions for the projectile. Shading indicates pressure of gas trapped in the void between projectile O-rings.

burst and sufficient projectile motion. By loading the narrow high-velocity projectiles in this way, we effectively maximize the quantity of gas that can pass around the projectile and create a cushion for two reasons: 1) the gas that is trapped between the O-rings remains at breech firing pressure, because after it is injected it is sealed by the rear O-ring; and 2) the volume in which the gas is trapped is much larger, because the narrow high-velocity projectile was designed with a smaller outer diameter to reduce the weight for a given wall thickness.

In addressing the above problems, we discovered another modification that had an effect on the amount of gas cushioning. Between gun firings, cleaning wads are accelerated down the barrel using compressed air. At one time, when a previous breech design was in use, a 6.35 mm diameter orifice had been drilled in the side of the barrel to provide a port through which compressed air could be injected (Fig. 5). When the present breech design was incorporated, another means of accelerating cleaning wads was developed and the orifice was plugged externally. Since the inner face of the plug was not flush with the inner surface of the barrel, the resulting cavity provided a route by which the compressed gas could escape past a projectile O-ring (Fig. 6). The severity of this effect was aggravated by the fact that it occurred at the breech end of the barrel, where the projectile velocity is slowest and the driver pressure is highest. In configurations where breech gas was injected into the projectile void, this release of gas occurred when the first O-ring passed

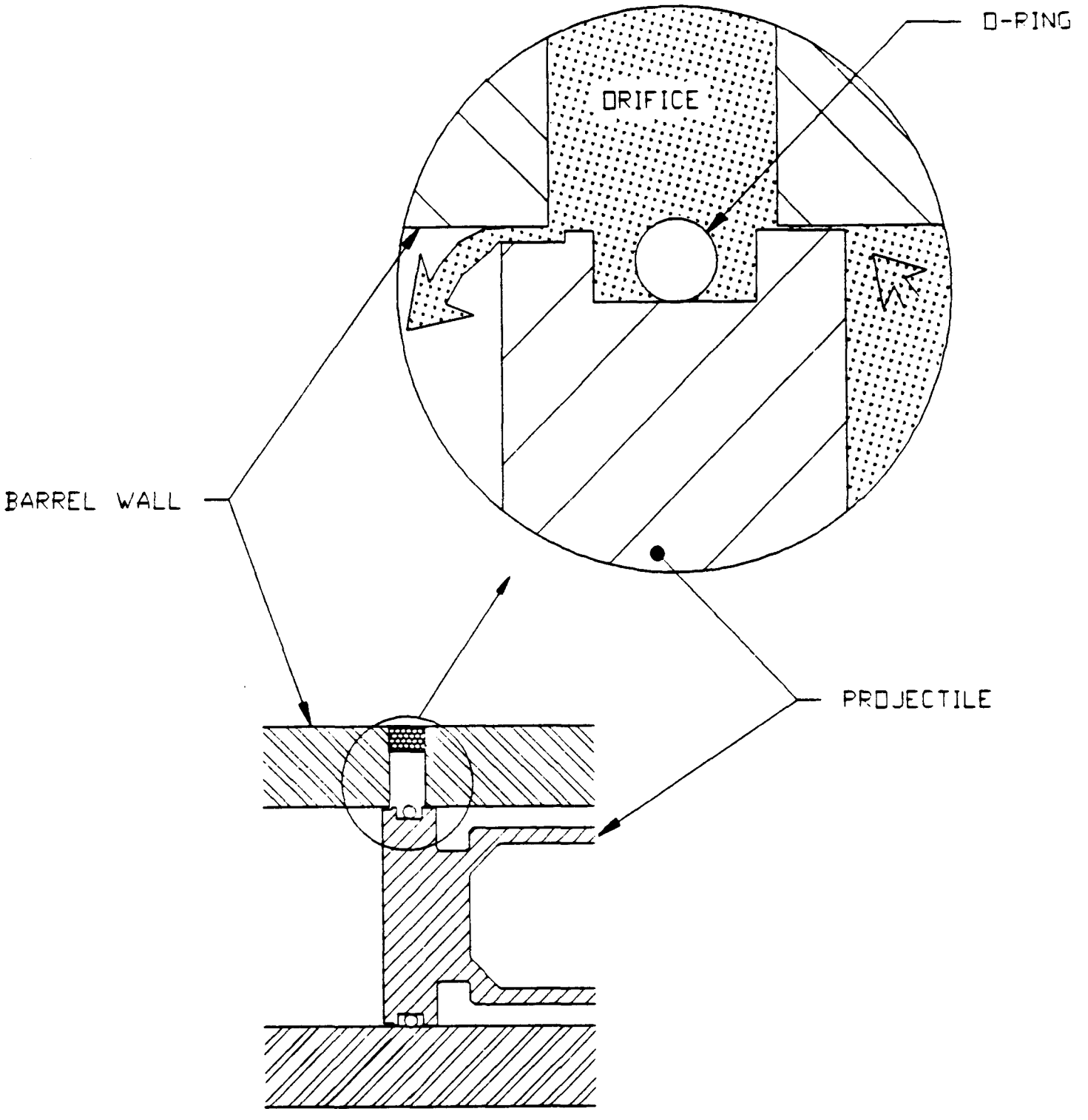


Fig. 6 Schematic representation of loss of sealing capability of a projectile O-ring as it moves past an open orifice in the side of the barrel. Arrows show resulting gas motion.

the orifice as illustrated in Figure 6, and the released gas remained in front of the projectile for the entire 25 m length of the barrel. It is worth noting that the rear projectile O- ring seal was also broken momentarily as it passed over the orifice.

## III. Solutions to the Problem

We have made minor modifications in: 1) the mode of operation, 2) the high-velocity projectile design, and 3) the gun itself, to control the presence of precompression. The primary change was to attach a tongue to the breech pilot plug to change the initial position of the projectile in the barrel. Placing the projectile in the position illustrated in Fig. 5b, with the rear O-ring forward of the breech taper, prevents the high pressure breech gas from being injected between the O-rings of the projectile. Since the projectile is placed in the barrel under ambient conditions, the void volume between the projectile O-rings is still filled with one atmosphere of air. The additional problem of gas leaks when the O-rings pass the orifice still exists, also. The latter problem can be overcome by placing the projectile at the position in Fig. 5d, but there is still an atmosphere of air in the projectile void. Our solution was to fill the orifice with a potting compound flush with the inner surface of the barrel, and drill a smaller (1.02 mm) diameter hole so that the air can be pumped out of the projectile

void when it is placed in the position depicted in Fig. 5c, with one O-ring on each side of the port. The purpose of the smaller orifice diameter is to prevent the O-ring from losing its seal when it passes over the orifice.

The initial configuration shown in Fig. 5c prevents precompression when the narrow high-velocity projectile is used, as long as the 63.5 mm spacer is not used at the muzzle. For experiments requiring the spacer, a new high-velocity projectile design was needed which was long enough so that the rear O-ring remained in the barrel at the time of impact. The new "wide high-velocity" projectile is shown in Fig. 3d. The large outer diameter was used to minimize the volume of the void and therefore minimize the amount of gas that can be carried by the projectile. The added width and length of this new projectile increase its weight, so the highest achievable velocity is somewhat lower than that for the narrow high-velocity version.

## IV. Experimental Verification

A number of diagnostic experiments (test shots) were fired to assess the problem and determine the relative effects of the various contributing factors. Quartz stress gauge experiments were performed to measure the magnitude of the stress at the target impact interface prior to projectile impact (shot conditions are listed in Table 2). For the full-electrode,

Table 2. Quartz Guage Experiments

| Shot | Velocity (km/sec) | Proj. Type(a) | Spacer | Proj. Posn.(b) | Comments |
|---|---|---|---|---|---|
| 2212 | 1.324 | b | no | a | |
| 2213 | 1.317 | b | yes | a | |
| 2214 | 1.328 | b | yes | a | |
| 2215 | 1.317 | b | yes | a | fluorocarbon elastomer O-rings |
| 2216 | 1.333 | b | yes | a | ethylene propylene O-rings |
| 2221 | 1.326 | b | no | a | |
| 2222 | 0.820 | a | yes | a | |
| 2223 | 1.023 | e | yes | a | |
| 2224 | 1.179 | b | yes | a | weighted projectile |
| 2227 | 0.406 | a | no | a | |
| 2238 | 1.345 | b | yes | b | |

Notes: Nitrile (Buna-N) O-rings were used in all cases unless otherwise noted. Aluminum projectiles carried no flyer plates. Orifice diameter was 6.35 mm for all shots.
(a) letters refer to projectile types displayed in Fig. 3
(b) letters refer to positions shown in Fig. 5.

shunted quartz gauges we used, the stress measurements are calibrated to stresses up to 2.5 GPa. At higher stresses, there is distortion in the measured waveform due to conduction [4]. Radiation pyrometer experiments were also carried out to determine the temperature and brightness of the gas cushion, and the degree to which it was mitigated by our efforts (shot conditions are listed in Table 3). In Figures 7-9, the time-resolved stress histories obtained in the quartz gauge experiments are plotted at different scales. Experiment 2227 comes closest to the ideal case of a step function. A standard projectile was fired at low velocity, and a breech pressure of only 4.65 MPa was required. No spacer was in place at the muzzle, so most of the mechanisms that we expect to contribute to the gas cushion are absent.

Experiments 2212 and 2221 were carried out without a 63.5 mm spacer on the muzzle. In both cases the narrow high-velocity projectiles (Fig. 3b) were used. They were launched close to their maximum velocity of about 1.33 km/sec. From Figures 7-9 one can see that, although the gas cushion is small, it still exists. The stress at the front surface of the quartz gauge becomes measurable some 0.2 ms before impact, and ramps up to approximately 0.5 GPa.

The question of whether O-ring effects are a contributing factor was addressed first because there had been a previous change from fluorocarbon elastomer (Viton: Parker Seals #V747-75) to nitrile O-ring composition and there was some uncertainty

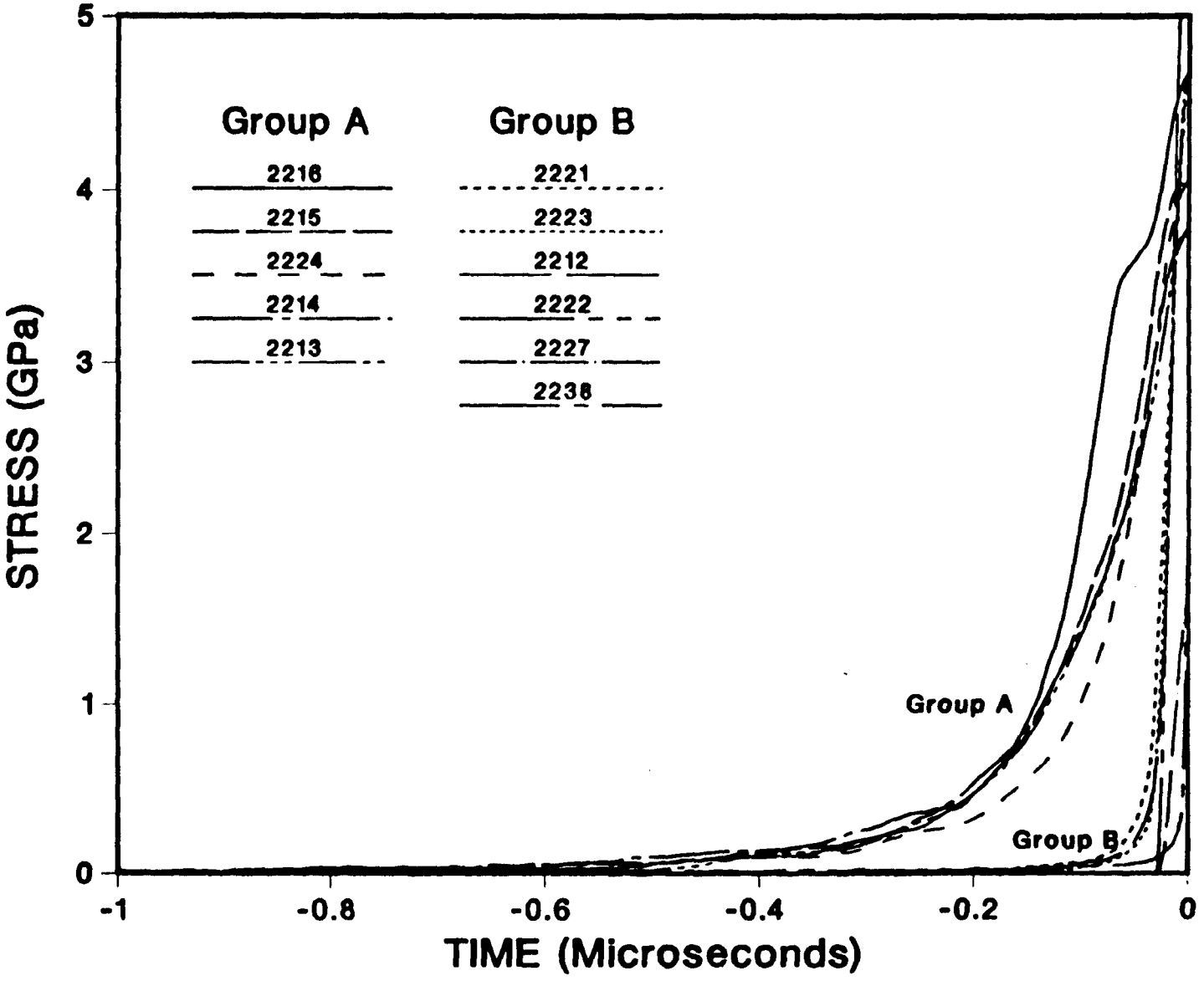


Fig. 7 Time-resolved axial stress at impact interface measured in quartz gauge experiments. Group A consists of experiments that experienced large precompression. Group B exhibited little or no precompression. Time scale is referenced approximately to impact.

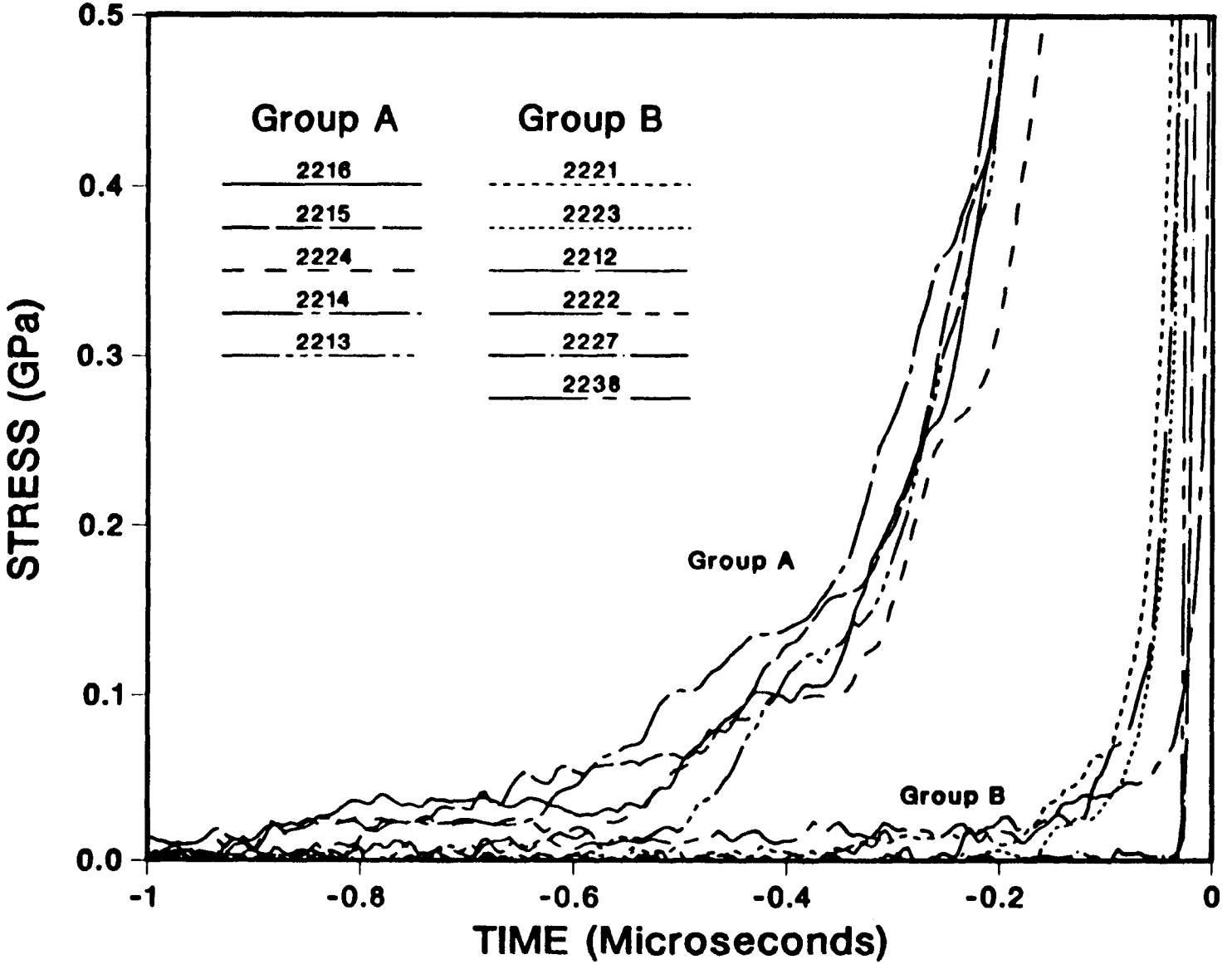


Fig. 8 Same as Figure 7 with expanded ordinate scale.

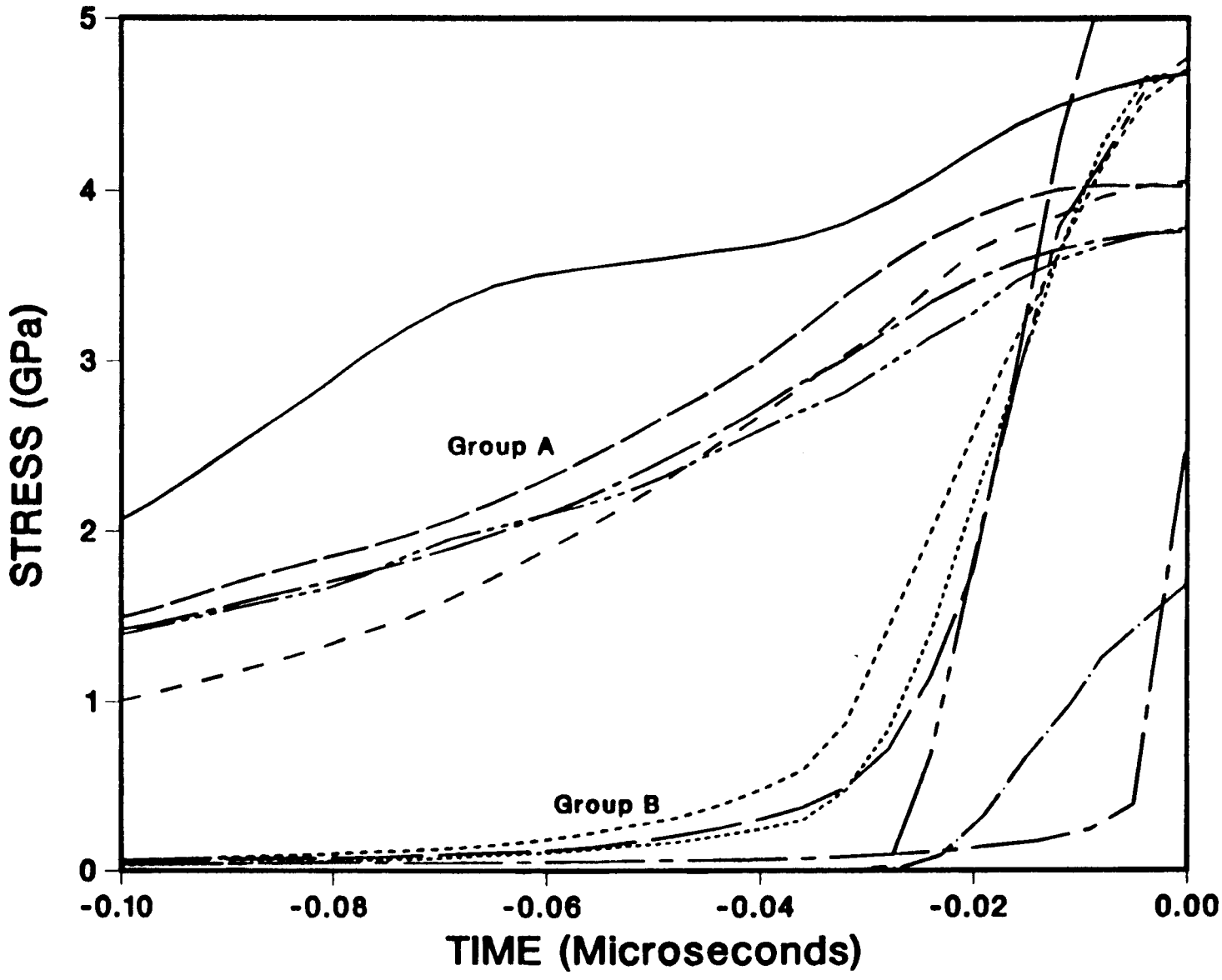


Fig. 9 Same as Figure 7 with expanded abscissa scale, for legend refer to previous figures.

about the effect of this change. We conducted identical experiments using nitrile, fluorocarbon elastomer, and ethylene propylene (Parker Seals #E540-80) O-rings. Another question was whether the O-ring gland tolerances were critical. We concurrently addressed this by varying the gland diameter by 0.05 mm increments. For experiments 2213, 2214, 2215 and 2216 the gun was in the same configuration as 2212 and 2221, except that a 63.5 mm spacer was in place between the barrel and target. All four shots were fired near the maximum velocity, and the large gas cushions observed in all cases were almost identical. The precompression stress is already measurable 0.8 ms before impact, and reaches nearly 4 GPa at impact. Thus, the material near the impact surface of the target never experiences a shock wave, but is gradually compressed by a ramp wave having a several hundred ns rise time. The only difference in firing conditions among the four experiments was the O-ring material (Table 2) and O-ring gland dimensions. The fact that the loading paths were nearly the same indicated that gas cushions of this magnitude are not a result of O-ring failure due to ablation or tolerances. To further address any questions about O-ring performance, these experiments should be repeated in a configuration that minimizes precompression from all other sources.

In experiments 2222 and 2223, the effect of projectile design was addressed. Both experiments made use of 63.5 mm spacers, with the projectile starting from the position shown in (Fig. 5a). In 2222 the standard projectile was used, and the gas cushion is absent. In 2223, a shortened version of the standard projectile

was used, and we observed a weak precompression disturbance similar in magnitude and duration to 2212 and 2221. Since the rear O-ring of the shortened standard projectile extends into the breech taper, but the projectile void volume is less than that of the narrow high-velocity projectile, its use gives rise to a gas cushion that is smaller than that observed for the narrow high-velocity projectile.

Experiment 2224 demonstrates that very large gas precompressions can be achieved at lower than maximum velocity. A narrow high-velocity projectile was weighted to 486 g to give a slower velocity, and fired from the position in Figure 5a using maximum breech pressure. The stress history for this case (Figures 7-9) shows the onset of precompression 0.8 ms before impact with a gradual rise up to the maximum.

In experiment 2238, the narrow high-velocity projectile was pushed forward to the starting position in Figure 5b to test the hypothesis that driver gas at breech pressure, carried in the projectile void, provides the dominant contribution to the gas cushion at impact. Figures 7-9 show that, indeed, the stress from the gas cushion in this case is not significant until about 0.2 ms before impact, and rises only to about 0.4 GPa before impact. Thus, preventing gas at breech pressure from filling the projectile void significantly reduces the amount of gas precompression.

A series of radiation pyrometry experiments was undertaken to determine the temperature and spectral radiance of the precompressed gas, and to continue examining the effect with more

sensitive diagnostics. Table 3 lists the pyrometer experiments and the corresponding gun configurations. In all cases the target consisted of a LiF window, which was impacted directly (except 2177 and 2178, in which 3.1 mm thick copper driver plates were glued on the front surface). The precompression flash was first observed in experiments 2173 and 2174, which were originally intended to determine if there is any measurable light emission from shocked LiF. The LiF targets had 300 nm thick vapor-deposited nickel layers which were supposed to mask any light emission from the barrel gas prior to impact. Well before impact, signals from all four channels of the pyrometer (representing four wavelength intervals in the visible and near-infrared) went off scale on the recording digitizers (see Figures 10-12 for spectral radiances at 569 nm wavelength, plotted at various scales). Pyrometer calibrations show that the minimum temperature required to achieve these signal levels from a blackbody is about 4000 K. Actual temperatures are probably significantly higher since the intensities were increasing at a rapid rate at the time they went off scale. The observation of intense thermal radiation implies that the opaque nickel film was vaporized by the compressed gas, forming a dense plasma just prior to impact.

Table 3. Radiation Pyrometer Experiments

| Shot | Velocity (km/sec) | Proj. Type[a] | Flyer | Proj. Posn.[b] | Orifice diam. (mm) | Comments |
|---|---|---|---|---|---|---|
| 2173 | 1.172 | b | Cu | a | 6.35 | Ni coating |
| 2174 | 1.183 | b | Cu | a | 6.35 | Ni coating |
| 2177 | 1.179 | b | Cu | a | 6.35 | Cu driver; Ni coating |
| 2178 | 1.174 | b | Cu | a | 6.35 | Cu driver; Ni coating |
| 2255 | 1.335 | b | none | b | 6.35 | |
| 2264 | 1.337 | b | none | c | 6.35 | void evacuated[c] |
| 2265 | 1.335 | b | none | c | 6.35 | void evacuated |
| 2266 | 1.287 | c | Al | d | 6.35 | |
| 2267 | 1.024 | e | thermite | c | 1.02 | void evacuated |
| 2268 | 1.027 | e | Ni/Al | c | 1.02 | void evacuated |
| 2272 | 1.267 | c | Ni/Al | c | 1.02 | void evacuated |
| 2273 | 1.274 | d | Ni/Al | c | 1.02 | void evacuated |
| 2282 | 1.026 | b | none | c | 1.02 | void evacuated |

Notes: 63.5 mm spacer was used for all shots
Nitrile (Buna-N) O-rings were used in all shots
(a) letters refer to projectiles displayed in Fig. 3
(b) letters refer to positions shown in Fig. 5
(c) valve to post-projectile volume was left open

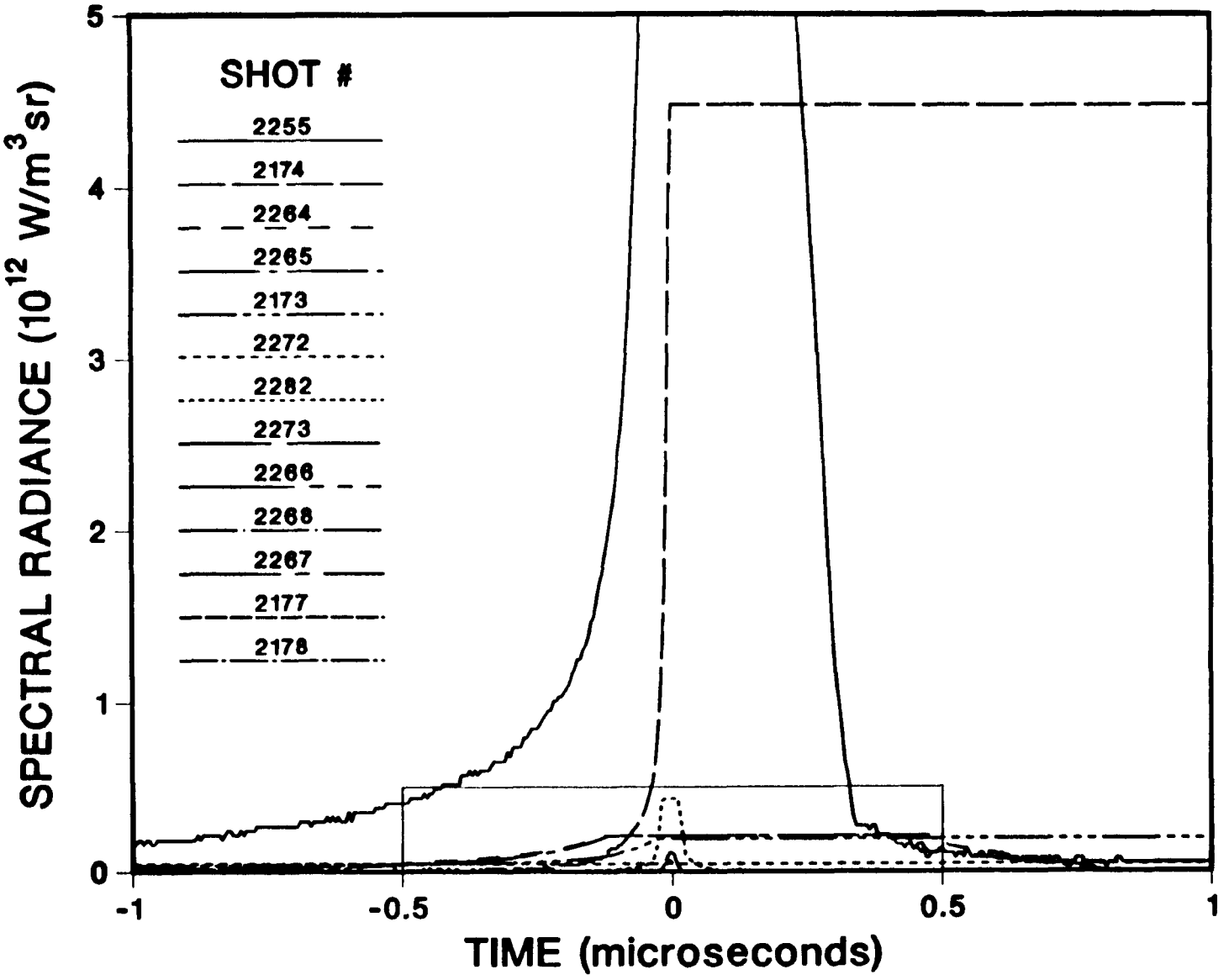


Fig. 10 Time-resolved spectral radiances from gas precompression flash measured by 569 nm channel of radiation pyrometer. Horizontal portion of a record indicates off-scale digital recorder. Experiment numbers in legend are arranged in approximate descending order of spectral radiance (note that many are too low to be resolved at this scale). Rectangular area at bottom center refers to expanded range of Figure 11. Time scale is referenced approximately to impact.

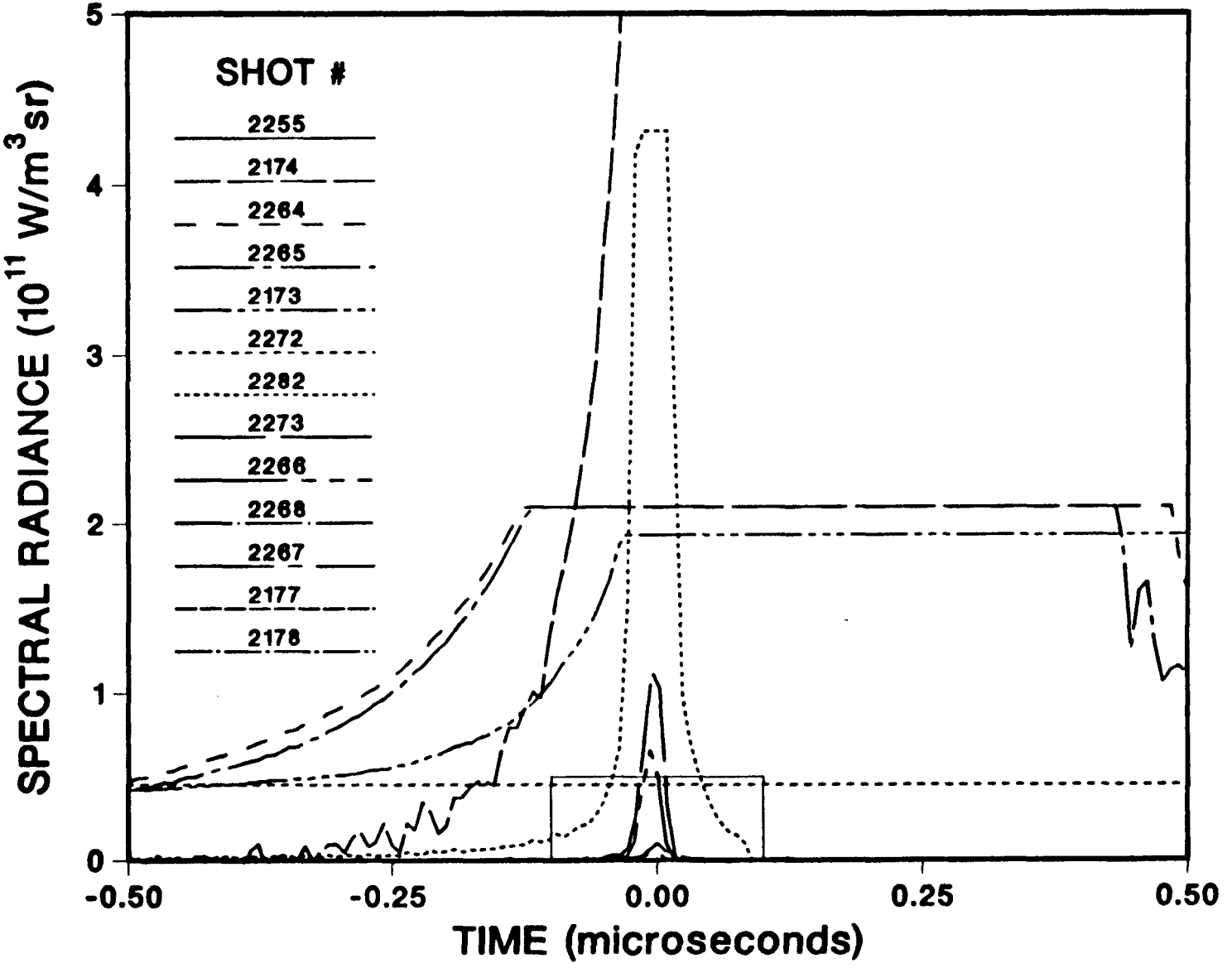


Fig. 11 Same as Figure 10 with expanded scale. Rectangular area at bottom center refers to expanded range of Figure 12.

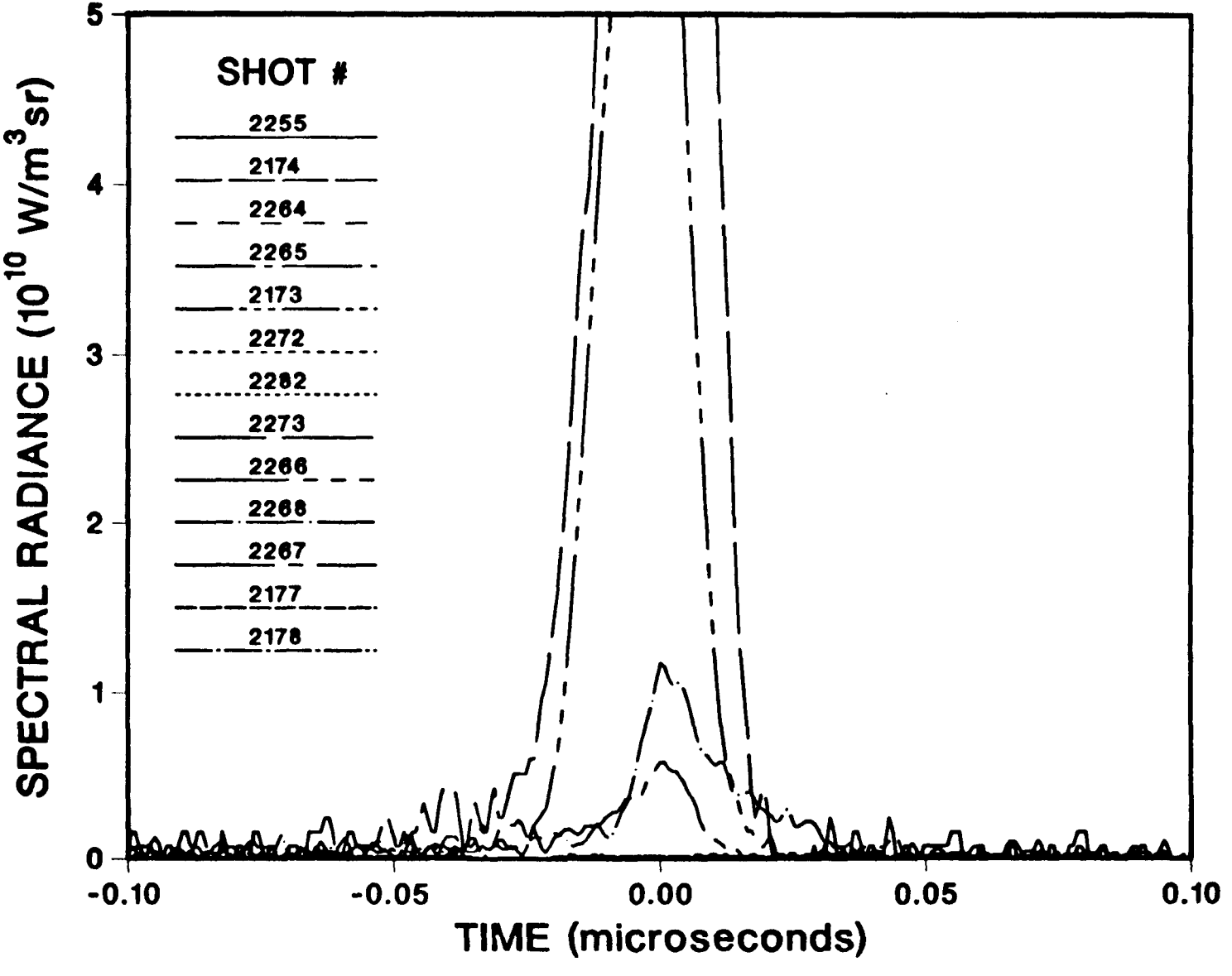


Fig. 12 Same as Figure 10 with expanded scale. Note that 2177 and 2178 are too weak to be seen even on this sensitive scale.

Experiments 2177 and 2178 were carried out under identical conditions, except that the LiF targets were masked by 3.1 mm thick copper driver plates to insure that the precompression flash would remain blocked from view. There was no measurable emission of light from these experiments (even on the most sensitive scale, see Fig. 12), demonstrating that: 1) LiF does not emit light at these shock levels, and 2) the presence of the opaque copper driver plates is sufficient to mask even the largest precompression flash.

Experiments 2255, 2264, 2265, and 2282 all made use of the narrow high velocity projectile in various initial configurations. In 2255, the projectile was inserted past the breech taper (Fig. 5b). Fig. 10 shows that the flash reaches the same brightness levels as for 2174 before going off scale, but the onset is earlier and the duration is shorter. The earlier onset is certainly due to the fact that the LiF target had no coating in experiment 2255. In the other experiments, it took time for the high temperature gas to heat the nickel layer to incandescence, but shot 2255 allows an unobstructed view of the hot gasses. The shorter duration is evidence that the impact interface cools more quickly, suggesting that less heat was deposited. This is consistent with a smaller gas cushion, an expected result of the different firing configuration.

For experiments 2264 and 2265 the orifice was converted to an evacuation port by connecting it to the same vacuum system used to evacuate the post-projectile volume. These two shots were

fired with the projectile in the position in Fig. 5c and the void evacuated. In 2264 the valve between the barrel orifice and the post-projectile vacuum was left open; in 2265 it was closed before firing. Despite this difference, the amount of light radiated from the compressed gas was almost identical (see Fig. 11). Since the signals went off the digitizer scale, the peak spectral radiances were not measured. However, the early part of the signals are an order of magnitude smaller than for experiment 2255 (see Fig. 10).

The larger precompression flash observed in experiment 2255 can only be explained by air at one atmosphere getting in front of the projectile by the mechanism illustrated in Fig. 6. In experiments 2264 and 2265, driver gas at much higher pressure escaped past the rear O-ring into the projectile void, but the resulting precompression flash was smaller. The fact that the same amount of light was observed in experiments 2264 and 2265 implies that the driver gas leaks past the rear O-ring seals as fast as it can pass through the vacuum line, the open valve, and enter the projectile void in experiment 2264. Experiment 2282 repeats the conditions of 2265, with a lower breech pressure and lower impact velocity. In addition, the evacuation port diameter had been reduced from 6.35 to 1.02 mm, preventing gas blowby past the O-rings. As expected, the precompression flash is much weaker and shorter in duration as the higher velocity shots (see Fig. 11; note that the digitizer setting was less sensitive for

this experiment, so the spectral radiance reaches a higher level before going off scale).

To test the effect of preventing driver gas from passing the projectile at the muzzle in a high velocity shot, we performed experiment 2266 using the teflon projectile depicted in Fig. 3c [5]. This projectile was borrowed from another gun facility, and its outer diameter was slightly undersized, but its greater length satisfied our requirement that the rear O-ring remains in the barrel at the time of impact, when the 63.5 mm spacer is in use. The projectile was loaded into the position shown by Fig. 5d, with both O-rings ahead of the evacuation port. Figures 11 and 12 show that the total duration of the flash was reduced to less than 50 ns and the peak intensity was down by another order of magnitude. Most importantly for shock temperature measurements, the light emission returns to zero within about 50 ns, at the end of the flash (i.e., there is no measurable light output at the end of the spike in emission). Thus, the gas cushion effect is negligible for this experimental configuration when measurements can be made more than 50 ns after impact. The precompression flash is small enough that reverse-ballistic, shock temperature measurements can be made, and (after 50 ns) light from compressed barrel gas will not interfere with longer-duration light from shocked material mounted on the face of a projectile that impacts a transparent window.

Shot 2272 also made use of the lighter teflon projectile to achieve a higher velocity for a reverse ballistic temperature

measurement. It was loaded in the position depicted in Fig. 5c, and the void was evacuated. Unexpectedly, we observed an extremely large precompression flash: the signal went off scale quickly and remained off scale during the recording interval of the digitizers (due to the sensitive setting, the spectral radiance at which the scale was exceeded was relatively low). The problem apparently returned due to a different mechanism related to the undersized diameter of the projectile. After the projectiles are loaded into the barrel and the breech is closed, the volume behind the projectile is evacuated prior to evacuation of the volume of the barrel ahead of it. This assures proper contact between the projectile and the breech pilot plug under normal conditions. However, the extension tongue we had attached to the breech pilot plug made contact with the teflon projectile on the curved radial part of the tail end (Fig. 3c). Thus, when the projectile is forced back against the tongue by the air in the barrel, it is also forced radially against one side of the barrel. Since the teflon projectiles are slightly undersized, this forced misalignment can prevent the O-rings from sealing properly on the opposite side, and driver gas can escape past the projectile and generate the observed precompression flash.

The first reverse-ballistic temperature experiments on reactive materials were shots 2267 and 2268, on pellets of thermite and nickel-aluminum, respectively. Since these were lower velocity shots, heavier projectiles (than the teflon) could be used, so the standard aluminum version was modified by

removing the rear 92 mm. The projectiles for these experiments were loaded in the position of Figure 5c, the void was evacuated and the valve was closed. Figure 12 shows that the precompression flash intensity is again reduced by another order of magnitude (virtually nonexistent within the sensitivity range of the pyrometer). The fact that the intensity returns to zero after the weak impact flash means that the shock temperature is too low to measure, and no significant exothermic shock-induced chemical reaction has taken place.

To prevent passage of driver gas around the high-velocity projectile at the muzzle, a new aluminum version was designed. Its length is great enough to satisfy our requirement that the rear O-ring is still inside the barrel at the time of impact in experiments where the 63.5 mm spacer is used. In addition, the design minimized potential problems of gas trapped in the annular void by keeping the outer diameter large. Unfortunately, the added length and diameter slightly increased the weight of the wide high-velocity projectile over the narrow version (by 6.8%), so its peak velocity is lower (by 2%).

Experiment 2273 was the first to make use of the new projectile (Fig. 3d). It was loaded in the position in Figure 5c and the void was evacuated. It was fired at maximum velocity, and carried a nickel-aluminum pellet for a reverse-ballistic temperature measurement. Figures 10-12 show that the impact flash is again of short duration (less than 50 ns) but its intensity is greater than that for 2267 and 2268, probably due to

the higher impact velocity. Since the intensity rapidly returns to zero, reverse-impact shock-temperature measurements can be made using this configuration. In this particular experiment, the temperature is below the threshold for measurement, so no observable shock-induced reaction has taken place.

This series of experiments also attests to the usefulness and sensitivity of light emission measurements. It is interesting to note that the smallest precompression observed with a quartz gauge (2238) was an experiment performed in the same configuration that led the the largest precompression in terms of spectral radiance (2255). In both cases a narrow high-velocity projectile (Fig. 3b) was fired from the position of Fig. 5c, at maximum velocity. Measuring light emission allowed us to find a way to reduce the gas precompression by three more orders of magnitude in spectral radiance, after having reduced it by orders of magnitude in stress.

## V. Applications of Gas Precompression

So far, all our discussion has been on the subject of understanding and eliminating mechanisms that can produce a gas cushion. There are a number of potential applications, however, in which the precompression is desirable. By using a narrow-bodied projectile in the initial position of Fig. 5b, a large void volume can be filled to any pressure with any type of gas.

In this way, the amount and character of the gas cushion can be controlled.

One application is to dynamically compress granular high explosives at a slower loading rate than achieved through shock compression, thereby minimizing the generation of "hot spots" where ignition occurs. By inhibiting the onset of chemical decomposition, non-reactive thermodynamic states can be observed at much higher pressures than in shock-loading experiments. This fact has been utilized by Setchell and Taylor [6] to examine high-pressure shock Hugoniot states in the explosive hexanitrostilbene (HNS). Figure 13 shows that when HNS is compressed more gradually to 8 GPa by taking advantage of precompression by the driver gas, the onset of the growth-to-detonation process is significantly delayed.

Similarly, by intentionally generating a high pressure gas cushion, samples can be quasi-isentropically compressed to achieve high dynamic pressures without the associated higher temperatures and lower peak densities produced by shock compression. The approach of Barker et al. [7,8] is to fill the entire barrel (two-stage gun launch tube) with a partial atmosphere of helium gas before firing the gun. This has several disadvantages: 1) the projectile encounters gas resistance the entire length of the barrel, so the final velocity is lower that it would be otherwise. 2) the first weak shock arrives at the impact interface hundreds of ms before impact, so wave motions that can alter one dimensional (uniaxial strain) conditions in

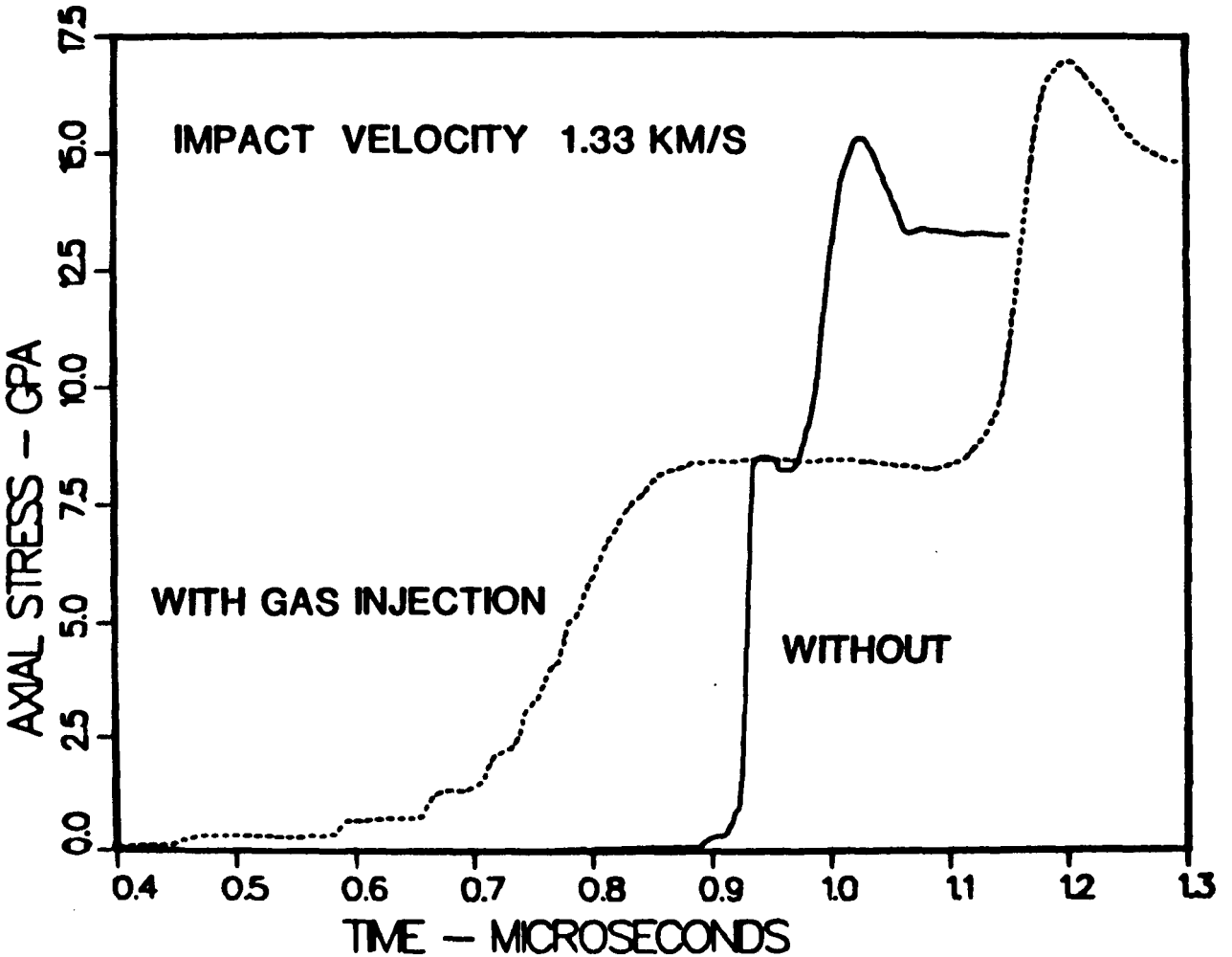


Fig. 13 Axial stress for two reverse impact experiments on HNS, with and without precompression. The presence of precompression delays the pressure buildup due to chemical energy release. The two stress histories have been shifted in time to facilitate comparisons.

the target have a long time to act, and 3) the projectile does mechanical work on the compressed gas for the entire length of the barrel, so the gas can reach extremely high temperatures. This fact, combined with the long contact time with the target, creates the possibility that the sample will experience significant heating due to thermal transport from the high temperature gas (or plasma).

Our observations indicate that an alternative would be to carry high pressure gas with the projectile, and release it in a manner similar to what we have observed just prior to impact by allowing the projectile to pass through a barrel expansion. While this method may reduce or overcome the above-listed disadvantages of filling the barrel, it may have its own disadvantages. It may be difficult to ensure that the compressed gas produces laterally uniform wave motion (uniaxial strain) in the target. Also, even though the technique may be easy to utilize on a single stage gas gun, it may not be practical on a hypervelocity two-stage gun.

The extremely high continuum emission observed in experiments 2173 and 2174 could provide a light source for transmission spectroscopy. While emission spectroscopy has been actively examined as a probe of shock-compressed materials, not all substances radiate sufficiently strongly to be studied in this way. In order to undertake transmission spectroscopy, a strong light source is necessary. Several workers have made use of powerful xenon flash lamps, directing the light into the sample

and reflecting it off an internal mirror (see, for example [9,10]). Another approach has been to attach a flash lamp to the projectile (e.g. Ogilvie and Duvall, [11]). We propose that the flash of the precompressed gas--particularly when enhanced by contact with a vapor-deposited layer that can be heated to a dense plasma--would make an ideal continuum source for transmission spectroscopy in shocked materials. By vaporizing and ionizing a metal layer, the optical depth (and emissivity) of the light source is higher, resulting in more intense and spectrally uniform radiation. In addition to its extremely high spectral radiance over a broad range of wavelengths, the timing and duration of the source is an inherent feature of the impact configuration.

The high gas pressures at the impact interface associated with the precompression also can give another dimension to shock recovery experiments. In gas gun recovery experiments lacking precompression, the sample is typically evacuated, or exposed to air at one atmosphere, prior to impact. The contribution of small amounts of ambient gasses to any chemical reaction that takes place is usually assumed to be minimal. The ability to generate the presence of a specific gas at high pressures and temperatures introduces a new dimension for shock recovery experiments aimed at studying shock-induced chemical reactions. For example, adjustment of oxygen fugacity (a measure of chemical activity that is a function of pressure, temperature and concentration of a given species) would be expected to shift the

equilibrium conditions and perhaps give rise to different recovered phases when shock recovery experiments are conducted.

## VI. Conclusions

There are a number of mechanisms that can lead to gas becoming trapped between a gun-launched projectile and a target, generating a high-pressure and high-temperature cushion prior to impact. We have learned that care must be taken when making modifications to gun operations so that precompression effects are not introduced. For many types of experiments, the precompression and/or heating of the sample by the resulting gas cushion is undesirable. There are some cases, however, where a controlled precompression may be useful. These applications include high-explosive Hugoniot experiments, quasi-isentropic compression experiments, and certain shock recovery experiments.

## VII. Acknowledgments

We appreciate the help of D. W. Dugan in supplying the lightweight teflon projectiles from the Sandia 2514 gun facility.

## References


[1] S. Thunborg, Jr., G.E. Ingram and R.A. Graham, "Compressed Gas Gun for Controlled Planar Impacts Over a Wide Velocity Range", Rev. Sci. Instrum., 35, (1964), pp. 11-14.

[2] R.E. Setchell, "Sandia 25-meter compressed Helium/Air Gun", in Shock Waves in Condensed Matter--1981, W.J. Nellis, L. Seaman and R.A. Graham, eds., (1982), pp. 657-660.

[3] R.E. Setchell and J.A. Guzman, "Barrel Vacuum Characteristics of the 26-Meter Helium/Air Gun", Sandia Internal Memorandum RS 5131/1067, (1978).

[4] R.A. Graham, F.W. Neilson, and W.B. Benedick, "Piezoelectric Current from Shock-Loaded Quartz--A Submicrosecond Stress Gauge", J. Appl. Phys, 36, (1965), pp. 1775-1783.

[5] S.A. Sheffield and D.W. Dugan, "Description of a New 63-mm Diameter Gas Gun Facility", in Shock Waves in Condensed Matter, Y.M. Gupta, ed., (1986), pp. 565-570.

[6] R.E. Setchell and P.A. Taylor, "A Refined Equation of State for Unreacted Hexanitrostilbene", J. Energetic Materials, (1988), in press.

[7] L.M. Barker, T.G. Trucano, J.R. Asay and J.L. Wise, "Preliminary Considerations for the Gasdynamic Precompression of Solid Molecular Hydrogen", Sandia National Laboratories, Report SAND85-0111, (1985).

[8] L.M. Barker, T.G. Trucano, J.L. Wise and J.R. Asay, "Experimental Technique for Measuring the Isentrope of Hydrogen to Several Megabars", in Shock Waves in Condensed Matter, Y.M. Gupta, ed., (1986), pp. 455-460.

[9] T. Goto, T.J. Ahrens, G.R. Rossman and Y. Syono, "Absorption Spectrum of Shock-Compressed $Fe^{3+}$-Bearing MgO and the Radiative Conductivity of the Lower Mantle", Phys. Earth Planet. Int., 22, (1980), pp. 277-288.

[10] C.S. Yoo, J.J. Furrer and G.E. Duvall, "Absorption Spectra and Reactions of Carbon Disulfide Under Shock Compression", in Shock Waves in Condensed Matter 1987, S.C. Schmidt and N.C. Holmes, eds, (1988), pp. 477-480.

[11] K.M. Ogilvie and G.E. Duvall, "Shock-induced changes in the electronic spectra of liquid $CS_2$", J. Chem. Phys., 78, (1983), pp. 1077-1087.

Distribution:

Mr. John Cable
CALSPAN Corporation/AEDC Division
Attn: Mr. Henry W. Ball
Mr. John Cable
von Karman Gas Dynamics Facility
Arnold Engineering Development Center
Arnold Air Force Station, TN 37389-9998

Mr. Gerald L. Winchenbach
Air Force Armament Laboratory
AFATL/FXA
Eglin AFB, FL 32542-5434

Mr. Ed Wittrock, Bldg I
Alcoa Laboratories
Aluminum Company of America
Alcoa Center, PA 15069

Mr. Don S. Randall
ASTRON Research and Engineering
130 Kifer Court
Sunnyvale, CA 94086

Department of the Army
Attn: Mr. Richard Audette
Mr. Ed Webster
HQ. USATC and Fort Dix
ARDC Test Site
Fort Dix, New Jersey 08640-5290

US Army Ballistics Research Laboratories
Attn: J. W. Evans
Bailey T. Haug
Rurik Loder
Aberdeen Proving Ground, MD 21005-5066

Dr. Henri Bernier
Commissariat a l'Energie Atomique
Centre d'Etudes de Limeil B.P. 27
94190 Villenueve-Saint-Georges
France

Pierre Chartagnac
Centre d'Etudes de Gramat
46500 Gramat, France

Dr. Jacques Charest
DYNASEN, Inc.
20 Arnold Place
Goleta, CA 93117

Mr. Gedeon Drouin
Defense Research Establishment
Val Cartier
P.O. Box 8800
Courcelette P.Q.
Canada GOA IRO

Dr. Alois Stilp
Ernst-Mach-Institut der Fraunhofer-Gesellschaft
Eckerstrasse 4
D 7800 Freiburg i. Br.
Federal Republic of West Germany

Mr. Wayne Hathaway, Rm. 1305
General Electric Co./Armament Systems Department
Lakeside Avenue
Burlington, VT 05402

Mr. William M. Isbell
Attn: Mr. William M. Isbell
A. C. Charters
General Research Corporation
5383 Hollister Avenue
Santa Barbara, CA 93160-6770

Dr. Niels K. Winsor
GT Devices, Inc.
5705A General Washington Drive
Alexandria, VA 22312-2408

Mr. Abraham Frydman
ERADCOM, Harry Diamond Laboratories
2800 Powder Mill Road
Adelphi, MD 20783

Mr. D. J. Krupovage 6585TG/TKE
6585th Test Group/TKE
Test Track Division
Holloman AFB, NM 88330

Honeywell Proving Ground
Attn: John A. Fitzgerald
Louis Lambert
23100 Sugar Bush Road
Elk River, MN 55330

Institut Franco-Allemand (ISL)
Attn: Dr. M. Giraud
Dr. F. Bauer
12 rue de l'Industrie
68301 Saint-Louis
France

Dr. Frederick Horz, MS-SN4
NASA Johnson Space Flight Center
Solar System Exploration, SN
Houston, TX 77058

Kuji Nemoto
Ordnance Development Center
The Japan Steel Works
1-2 Yurakucho 1-Chome
Chiyoda-Ku
Tokyo 100, Japan

DRSMC-LCA-G(D) Bldg. 382
Attn: Mr. Ted Gora
Mr. Grey Columbo
US Army Armament Research & Development Center
Dover, NJ 07801

Prof. Robert W. Courter
Mechanical Engineering Dept.
Louisiana State University
Baton Rouge, Louisiana 70803-6413

Dr. Garry Hough, M/S TH-85
LTV Aerospace and Defense Company
Vought Missiles and Advanced Programs
P.O. Box 650003
Dallas, TX 75265-0003

Maxwell Laboratories
Attn: Dr. M. Holland
Dr. R. Dethlefsen
8888 Balboa Avenue
San Diego, CA 92123

Dr. K. F. Leisinger
Wehrtechnische Dienstaelle Fuer
Waffen und Munition WTD91 Schiessplatz
4470 Meppen/EMS
Federal Republic of West Germany

Dr. Gary Chapman
NASA/Ames Research Center
Moffett Field, CA 94035

Mr. Andrew E. Williams, Code 7945
U.S. Naval Research Laboratory
Washington, DC 20375

Mr. Bill Holt
Naval Surface Weapons Center
Dahlgren, VA 22448

Mr. Richard D. Szczepanski
Orlando Technology, Inc.
Bldg. 5, Madak Office Center
60 Second Street
Shalimar, FL 32579

Dr. K. Kani
Okayama University
Faculty of Education
3-1-1 Tsushima-naka,
Okayama 700, Japan

Mr. Hallock F. Swift
Physics Application, Inc.
800 Britton Road
Dayton, OH 45429

Dr. R. R. Ijsselstein
Prins Maurits Laboratory, TNO
P.O. Box 45
2280 AA Rijswijk
The Netherlands

Mr. P. W. W. Fuller
Royal Armament Research and Development Establishment
Ballistics Branch R31
Ft. Halstead, Sevenoaks
Kent, TN 14 7BP U.K.

Mr. H. Ichikawa
Sagamihara Machinery Works
Testing and Research Department
Mitsubishi heavy Industries, Ltd.
3000 Tana Sagamihara,
Kangawa 229
Japan

Southwest Research Institute
Attn: C. E. Anderson
Alex B. Wenzel
6220 Culebra Road
San Antonio, TX 78284

Dr. E. Igenbergs
Institut Fuer Luft und Raumfahrt
Technische Universitaet
8000 Muenchen 2
Arcisstrasse 21
Federal Republic of Germany

Stephen Bless
University of Dayton Research Institute
300 College Park Drive
Dayton, OH 45469

Dr. George Bishop
US Army - Materials Laboratory
Director, Materials Reliability Directorate
SLCMT-MS
Watertown, MA 02172-0001

Raymond Zowarka
University of Texas
Center for Electromagnetics
10100 Burnet Road
Austin, TX 78712

Dr. Adam Bruckner
University of Washington
Aerospace and Energetic Research Program
Mail Stop FL-10
Seattle, WA 98195

Ian R. McNab
Westinghouse Electric Corp.
Mail Stop ED5
401 E. Hendy Avenue
P.O. Box 499
Sunnyvale, CA 94088

Dr. R. L. Pope
Weapons Systems Research Laboratory
Defence Research Centre
Aeroballistics Division
P.O. Box 2151
G.P.O. Adelaide
South Australia 5001

George Jepps
Weapons Systems Research Laboratory
Defence Research Centre
Aeroballistics Division
P.O. Box 2151
G.P.O. Adelaide
South Australia 5001

K-Tech Corporation
Attn: Dr. E. S. Gaffney
L. Lee
Tom Smith
Kirtland AFB, NM 87115

Dr. Naresh Thadhani
Center of Explosive Technology
New Mexico Tech
Socorro, NM 87801

Dr. M. F. Nicol
Dept. of Chemistry & Biochemistry
University of California
Los Angeles, CA 90024

M. Shahinpoor
University of New Mexico
Albuquerque, NM 87131

Tokyo Institute of Technology
Attn: K. Kondo
Dr. A. Sawaoka
Research Lab. Eng. Materials
4259 Nagatsuta, Midori
Yokohama 227
Japan

Washington State University
Attn: Y. M. Gupta
George Duvall
G. S. Yoo
Physics Department
Pullman, WA 99164-2814

California Institute of Technology
Attn: Epaprodito Gelle
T. J. Ahrens
Seismology Laboratory 252-21
Pasadena, CA 91125

J. W. Forbes
Naval Surface Weapons Center
White Oak
Silver Spring, MD 20910

W. J. Kolkert
Prins Maurits Laboratory
TNO P. O. Box 45
2280 AA Rijswijk
The Netherlands

Dr. D. P. Dandekar
Department of the Army
Army Materials and Mechanics
Research Center
Watertown, MA 02171

R. M. Schmidt
Post Office Box 3999
The Boeing Co.
Seattle, WA 98124

Los Alamos National Laboratories
Attn: J. N. Fritz
Mike Fletcher
A. C. Mitchell
S. C. Schmidt
Dennis Shampine, MS J970
John Shaner, MS J970
S. A. Sheffield
J. Wackerle
P.O. Box 1663
Los Alamos, NM 87545

Lawrence Livermore National Laboratory
Attn: Ron Hawke, L-35
H. B. Radousky
N. C. Holmes
Charles Honodel L-368
Bill Nellis, L-299
D. J. Steinberg
Allan Susoeff
M. Van Theil
P.O. Box 808
Livermore, CA 94550

Sandia Internal:
1100 F. L. Vook
1124 W. M. Trott
1150 G. A. Samara
1153 B. Morosin
1153 M. Boslough (20)
1153 R. A. Graham
1153 M. Lewis (2)
1153 M. Anderson (2)
1153 D. Wackerbarth (2)
1153 P. A. Taylor
1510 J. W. Nunziato
1520 L. W. Davison
1530 D. B. Hayes
1531 S. L. Thompson
1533 P. Yarrington
1534 J. R. Asay
1534 D. R. Ek
1534 D. E. Cox
1534 R. L. Moody
1534 L. M. Barker
1534 C. A. Hall
1534 R. D. Hardy

| | |
|---|---|
| 1534 | J. M. Miller |
| 1534 | L. C. Chhabildas |
| 1534 | D. E. Grady |
| 1534 | J. L. Wise |
| 1534 | C. H. Konrad |
| 1534 | M. D. Furnish |
| 2514 | D. W. Dugan |
| 2514 | L. J. Weirick |
| 2514 | P. L. Stanton |
| 2515 | J. L. Miller |
| 2515 | A. M. Renlund |
| 3141 | S. A. Landenberger (5) |
| 3151 | W. I. Klein (3) |
| 3154-1 | C. L. Ward (8)<br>For DOE/OSTI |
| 5164 | R. E. Setchell (4) |
| 6230 | W. C. Luth |
| 8524 | J. A. Wackerly |

Figure Captions

Fig. 1 VISAR record for experiment 2168, reverse impact of HNS on sapphire at 1.33 km/sec. The shock-Hugoniot relation for sapphire has been used to convert particle velocity to axial stress. Impact occurs at t = 0.

Fig. 2 Quartz gauge-measured axial stress histories for two experiments: one with a large precompression (2213), and the other with small precompression (2238). The only difference in firing conditions was the initial projectile position (see Table 1). Impact at t = 0.

Fig. 3 Cross sections of projectiles: a) "standard", b)"narrow high-velocity", c) "teflon", d)"wide high-velocity", and e) "shortened standard". Small arrows indicate positions of O-rings.

Fig. 4 (a) Configuration of gun with standard projectile in breech. Length of projectile prevents high-pressure driver gas from getting into space between O-rings. A "narrow high-velocity" projectile is shown at the muzzle with no spacer in place; the rear O-ring still seals at the time of impact. (b) Muzzle of gun with spacer in place. Rear O-ring of narrow high-velocity projectile is outside the barrel at impact.

Fig. 5 Cross-section of breech end of barrel, with four initial starting positions for the projectile. Shading indicates pressure of gas trapped in the void between projectile O-rings.

Fig. 6 Schematic representation of loss of sealing capability of a projectile O-ring as it moves past an open orifice in the side of the barrel. Arrows show resulting gas motion.

Fig. 7 Time-resolved axial stress at impact interface measured in quartz gauge experiments. Group A consists of experiments that experienced large precompression. Group B exhibited little or no precompression. Time scale is referenced approximately to impact.

Fig. 8 Same as Figure 7 with expanded ordinate scale.

Fig. 9 Same as Figure 7 with expanded abscissa scale, for legend refer to previous figures.

Fig. 10 Time-resolved spectral radiances from gas precompression flash measured by 569 nm channel of radiation pyrometer. Horizontal portion of a record indicates off-scale digital recorder. Experiment numbers in legend are arranged in approximate descending order of spectral radiance (note that many are too low to be resolved at this scale). Rectangular area at bottom center refers to expanded range of Figure 11. Time scale is referenced approximately to impact.

Fig. 11 Same as Figure 10 with expanded scale. Rectangular area at bottom center refers to expanded range of Figure 12.

Fig. 12 Same as Figure 10 with expanded scale. Note that 2177 and 2178 are too weak to be seen even on this sensitive scale.

Fig. 13 Axial stress for two reverse impact experiments on HNS, with and without precompression. The presence of precompression delays the pressure buildup due to chemical energy release. The two stress histories have been shifted in time to facilitate comparisons.